


**Strain- and pressure-tuned magnetic interactions in honeycomb Kitaev materials**Ravi Yadav,<sup>1</sup> Stephan Rachel,<sup>2</sup> Liviu Hozoi,<sup>1</sup> Jeroen van den Brink,<sup>1,3</sup> and George Jackeli<sup>4,5,\*</sup><sup>1</sup>*Institute for Theoretical Solid State Physics, IFW Dresden, Helmholtzstr. 20, 01069 Dresden, Germany*<sup>2</sup>*School of Physics, University of Melbourne, Parkville, VIC 3010, Australia*<sup>3</sup>*Department of Physics, Technical University Dresden, 01062 Dresden, Germany*<sup>4</sup>*Institute for Functional Matter and Quantum Technologies, University of Stuttgart, Pfaffenwaldring 57, D-70569 Stuttgart, Germany*<sup>5</sup>*Max Planck Institute for Solid State Research, Heisenbergstrasse 1, D-70569 Stuttgart, Germany* (Received 7 March 2018; revised manuscript received 31 August 2018; published 20 September 2018)

A range of honeycomb-lattice compounds has been proposed and investigated in the search for a topological Kitaev spin liquid. However, sizable Heisenberg interactions and additional symmetry-allowed exchange anisotropies in the magnetic Hamiltonian of these potential Kitaev materials push them away from the pure Kitaev spin-liquid state. Particularly the Kitaev-to-Heisenberg coupling ratio is essential in this respect. With the help of advanced quantum-chemistry methods, we explore how the magnetic coupling ratios depend on strain and pressure in several honeycomb compounds ( $\text{Na}_2\text{IrO}_3$ ,  $\beta\text{-Li}_2\text{IrO}_3$ , and  $\alpha\text{-RuCl}_3$ ). We find that the Heisenberg and Kitaev terms are affected differently: For strain, in particular, the Heisenberg component decreases more rapidly than the Kitaev counterpart. This provides a scenario where strain can stabilize a spin liquid in such materials.

DOI: [10.1103/PhysRevB.98.121107](https://doi.org/10.1103/PhysRevB.98.121107)

**Introduction.** The realization of quantum spin liquids (QSLs) in spin-orbit driven correlated materials is an intensively pursued goal in the condensed matter community, both experimentally and theoretically. In a QSL strong fluctuations prevent long-range magnetic order even at the lowest temperatures and instead a nontrivial ground state forms with long-range quantum entanglement between spins [1–3]. Of particularly great promise in this context is the Kitaev Hamiltonian on honeycomb lattices, which exhibits various topological spin-liquid phases [4]. The paramount attention given to such states can be understood by the fact that they are topologically protected from decoherence [5], display fractional excitations with non-Abelian exchange statistics, and therefore hold promise in the field of quantum information and quantum computation.

The quest for the physical realization of the Kitaev spin liquid for effective spin-1/2 sites took a big stride forward with the proposal of the honeycomb  $5d^5$  iridate materials as host of the Kitaev-Heisenberg model [6,7]. The latter describes the interactions between spin-1/2 moments with the help of two competing nearest-neighbor (NN) couplings, i.e., an isotropic Heisenberg term ( $J$ ) assumed to mainly arise from direct exchange between Ir-ion  $d$  orbitals and an anisotropic Kitaev component ( $K$ ) which stems from superexchange along the Ir-O-Ir paths.

Certain materials, in particular  $\text{Na}_2\text{IrO}_3$ ,  $\text{Li}_2\text{IrO}_3$ , and  $\alpha\text{-RuCl}_3$ , have been extensively studied experimentally in this context [8–19] as well as within the electronic-structure computational field, by either quantum-chemistry [20–23] or density-functional-based [24–28] methods. However, it turns

out that the anticipated QSL regime is precluded in these honeycomb compounds, most likely due to the presence of reasonably strong NN Heisenberg interactions, longer-range spin couplings, or the combination of both these factors: So far, all the measurements indicate magnetic long-range order at low temperatures and zero external magnetic field. None of these systems however exhibits the conventional Néel state although the magnetic ions form bipartite lattices in all of them. It has been suggested that these materials are still located in the phase diagram in close vicinity to the spin-liquid regime [13,14,16,18,19]. This has then inspired rigorous experimental effort to test their properties under strain or pressure [13,29–34]. In particular, there have been claims for finding the evidences of spin-liquid states under applied pressure in  $\beta\text{-Li}_2\text{IrO}_3$  [13,29],  $\gamma\text{-Li}_2\text{IrO}_3$  [30], and  $\alpha\text{-RuCl}_3$  [31]. It is worth noting that even more complex strain experiments have been suggested [35,36]. Very recently, the observation of a QSL has been reported in a hydrogen-intercalated iridate, with the QSL phase replacing the complex magnetic order of the parent compound [37].

Here we explore the effects of strain and pressure on the NN isotropic and anisotropic interactions by employing *ab initio* quantum-chemistry methods. We find that strain is more promising than pressure, in the sense that strong enhancement of the  $K/J$  ratio is obtained when expanding the in-plane lattice constants. In the case of hyperhoneycomb  $\text{Li}_2\text{IrO}_3$ , we also find strong variations of the symmetric off-diagonal  $\Gamma$  couplings:  $|\Gamma_{xy}|$  becomes significantly larger under pressure and might play an important role in shaping the magnetic properties of this material, as discussed in Refs. [33,38]. Looking at such trends gives a profound insight into the different competing processes coming into play for different compounds or structures and can provide guidelines or direction for further experimental investigations.

\*Also at: Andronikashvili Institute of Physics, 0177 Tbilisi, Georgia

*Qualitative analysis.* The Kitaev-Heisenberg Hamiltonian [7] originally proposed as a minimal model for the honeycomb-lattice iridates takes the following form on a given bond of NN's  $i, j$ :

$$\mathcal{H}_{ij}^{(\gamma)} = J \tilde{\mathbf{S}}_i \cdot \tilde{\mathbf{S}}_j + K \tilde{S}_i^\gamma \tilde{S}_j^\gamma, \quad (1)$$

where  $\tilde{\mathbf{S}}_i$  and  $\tilde{\mathbf{S}}_j$  represent pseudospin-1/2 operators for the ground-state Kramers doublets of  $\text{Ir}^{4+}$  (or  $\text{Ru}^{3+}$ ) ions, the first and second terms correspond to the isotropic Heisenberg interaction and the anisotropic Kitaev coupling, respectively, and  $\gamma \in \{x, y, z\}$  labels the three inequivalent bonds and the corresponding Cartesian components of the pseudospins. Depending on the  $K/J$  ratio, the model (1) is known to host a rich phase diagram containing the Kitaev spin liquid and a variety of ordered states [7,39]. For a qualitative description of pressure effects on the effective coupling constants  $K$  and  $J$ , we assume that under uniform pressure all interatomic distances rescale in the same way and consider only the leading contributions to the exchange interactions.

A perturbative analysis estimates that  $J \sim \frac{t_{dd}^2}{U}$  and  $K \sim -\frac{t_{pd}^4 J_H}{\Delta_{pd}^2 U^2}$  [6,7], with the Heisenberg term predominantly related to direct exchange while the Kitaev interaction is mostly due to superexchange processes along the Ir-O-Ir paths. Here,  $t_{dd}$  and  $t_{pd}$  stand for the hybridization amplitudes between  $d$  orbitals of neighboring Ir ions and between Ir  $d$  and O  $p$  states, respectively, and  $\Delta_{pd}$  is the charge-transfer energy. The interaction parameters  $U$  and  $J_H$  correspond to the on-site Coulomb repulsion and the Hund coupling, respectively. In the simplest picture, the hybridization amplitudes scale with the interionic distance  $r$  as  $t_{dd} \sim r^{-5}$  and  $t_{pd} \sim r^{-7/2}$  [40]. This, in turn, gives a rescaling of the coupling constants  $J = J_0(\frac{a}{a_0})^{-10}$  and  $K = K_0(\frac{a}{a_0})^{-14}$  when the characteristic interionic length scale changes from  $a_0$  to  $a$  under uniform pressure or strain.

The above estimates are based on the dominant subset of possible exchange processes and are thus rather rough in character. They suggest that the strengths of the NN isotropic and anisotropic coupling constants get differently renormalized under uniform pressure. In order to test this quantitatively we have performed electronic-structure calculations using many-body quantum-chemistry methods for variable interionic distances within a family of potential Kitaev spin-liquid materials. The trends found by *ab initio* quantum-chemistry calculations indicate in fact more subtle physics as compared to the simplified effective superexchange model.

*Electronic-structure calculations.* The transition-metal (TM) ions show octahedral ligand (L) coordination and form a honeycomb ( $\text{Na}_2\text{IrO}_3$  and  $\alpha\text{-RuCl}_3$ ) or hyperhoneycomb lattice ( $\beta\text{-Li}_2\text{IrO}_3$ ) in the oxides and the chloride discussed here, as shown in Fig. 1. The key structural difference between the honeycomb and hyperhoneycomb structures is that the Ir sites display a truly 2D network in the former while they form a slightly more complicated 3D arrangement in the latter, with alternate rotation of two adjacent B2 bonds around the B1 link [13] [see Fig. 1(b)].

In both  $\text{Na}_2\text{IrO}_3$  and  $\alpha\text{-RuCl}_3$ , a block of two NN octahedra displays  $C_{2h}$  point-group symmetry [41], which then allows a generalized bilinear Hamiltonian of the following form for a

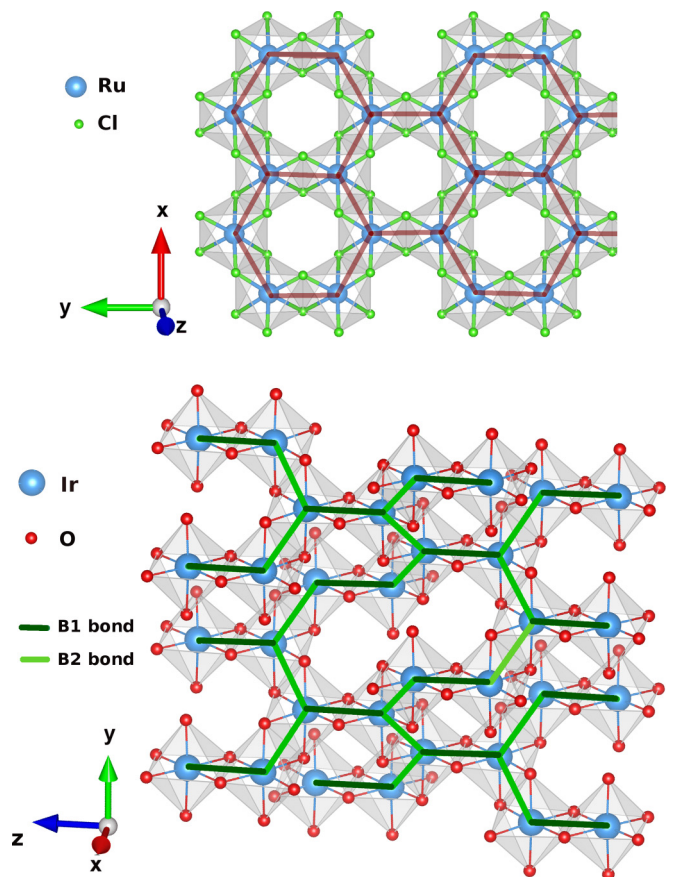


FIG. 1. (top) Ru-ion honeycomb lattice (blue) with Cl-ligand octahedral coordination (green sites) in  $\text{RuCl}_3$ . (bottom) Ir-ion hyperhoneycomb lattice in  $\beta\text{-Li}_2\text{IrO}_3$ . The local environment of the Ir sites remains similar to the 2D honeycomb network.

pair of pseudospins  $i$  and  $j$ :

$$\mathcal{H}_{ij}^{(\gamma)} = J \tilde{\mathbf{S}}_i \cdot \tilde{\mathbf{S}}_j + K \tilde{S}_i^\gamma \tilde{S}_j^\gamma + \sum_{\alpha \neq \beta} \Gamma_{\alpha\beta} (\tilde{S}_i^\alpha \tilde{S}_j^\beta + \tilde{S}_i^\beta \tilde{S}_j^\alpha), \quad (2)$$

where the  $\Gamma_{\alpha\beta}$  coefficients refer to off-diagonal components of the symmetric anisotropic exchange matrix, with  $\alpha, \beta \in \{x, y, z\}$ . An antisymmetric Dzyaloshinskii-Moriya (DM) interaction is not allowed, given the inversion center. On the other hand, a block of two NN octahedra in the hyperhoneycomb structure may display two different types of point-group symmetry: The *ab initio* data is mapped on the Hamiltonian (2) for the so-called B2 bonds since the deviations from  $C_{2h}$  point-group symmetry are tiny, while bond B1 features  $D_2$  point-group symmetry and allows DM antisymmetric anisotropic exchange in the effective spin Hamiltonian [21,33]. The latter can be then written for bond B1 as:

$$\begin{aligned} \tilde{\mathcal{H}}_{ij}^{(z)} = & J \tilde{\mathbf{S}}_i \cdot \tilde{\mathbf{S}}_j + K \tilde{S}_i^z \tilde{S}_j^z + \Gamma_{xy} (\tilde{S}_i^x \tilde{S}_j^y \\ & + \tilde{S}_i^y \tilde{S}_j^x) + \mathbf{D} \cdot \tilde{\mathbf{S}}_i \times \tilde{\mathbf{S}}_j. \end{aligned} \quad (3)$$

A local Kitaev reference frame is used here, such that for each TM-TM link the  $z$  coordinate is perpendicular to the  $\text{TM}_2\text{L}_2$  plaquette [ $\mathbf{D} = (D, D, 0)$  in this frame].

TABLE I. NN magnetic couplings (in meV) for bond B1 in  $\text{Na}_2\text{IrO}_3$  for variable Ir-Ir bond length  $a$ ; the relative change is  $\delta a = a/a_0 - 1$ . Results of spin-orbit MRCI calculations are shown.

$\delta a$	$a$ (Å)	$K$	$J$	$\Gamma_{xy}$	$\Gamma_{zx} = -\Gamma_{yz}$	$ K/J $
+2%	3.20	<b>-18.8</b>	<b>3.8</b>	-0.2	1.8	4.94
Expt.	3.14	<b>-20.8</b>	<b>5.2</b>	-0.7	0.8	4.00
-1.5%	3.09	<b>-24.6</b>	<b>5.9</b>	-1.3	1.1	4.17
-3%	3.04	<b>-28.9</b>	<b>6.8</b>	-2.3	1.5	4.25
-5%	2.98	<b>-34.7</b>	<b>7.7</b>	-3.4	2.1	4.51

Mapping of the *ab initio* data onto an effective spin Hamiltonian is carried out following the procedure earlier employed in Refs. [22,42,43]. Experimental lattice positions were used as reference in the many-body quantum-chemistry calculations, as reported for  $\text{Na}_2\text{IrO}_3$ ,  $\beta\text{-Li}_2\text{IrO}_3$ , and  $\alpha\text{-RuCl}_3$  in Refs. [11,13,44]. Structural data corresponding to -1.5%, -3%, -5%, and +2% modification of the bond lengths were additionally considered: For simplicity, we assumed here that the unit-cell parameters and all interatomic distances rescale the same way, except the case of +2% change, implying tensile strain. In order to realistically model strain, while stretching the in-plane lattice parameters ( $a$ ,  $b$ ) we simultaneously reduced by the same percentage the out-of-plane lattice constant ( $c$ ). A similar approximation provides quantum-chemistry data in good agreement with the experiment for the Heisenberg  $J$  in strained cuprates [45].

Hydrostatic pressure corresponding to the considered bond-length reductions seems to be feasible. For  $\text{RuCl}_3$ , a reduction of the Ru-Ru bond length by 5% requires pressure of 4 GPa [32]. We further assume that the required pressure for  $\text{Na}_2\text{IrO}_3$  will be similar as for  $\alpha\text{-Li}_2\text{IrO}_3$  (not considered in this paper), where 2.5 GPa was reported to yield 5% bond-length reduction [46]. For  $\beta\text{-Li}_2\text{IrO}_3$ , a somewhat slightly stronger pressure of 10.6 GPa is required to obtain the desired reduction of the bond lengths [29].

*Results.* We start our qualitative discussion with  $\text{Na}_2\text{IrO}_3$ . NN magnetic couplings as derived from spin-orbit multireference configuration-interaction (MRCI) calculations [47] are listed in Table I. For bond B1,  $K$  increases from -20.8 meV for the experimental crystal structure at ambient pressure to -34.7 meV on 5% reduction of the Ir-Ir bond length.  $J$ , on the other hand, displays a rather modest enhancement, from 5.2 to 7.7 meV. This translates in an increase of the  $|K/J|$  ratio from 4.0 to 4.5.  $\Gamma_{xy}$  and  $\Gamma_{zx}$  also gain significant strength with rising pressure but remain nevertheless one order of magnitude smaller than  $K$ .

As earlier reported [20,23,48], the effective couplings on bonds B1 and B2 may differ significantly. The main distortion in honeycomb iridates and  $\text{RuCl}_3$  is trigonal compression of the ligand cages. However, in addition to trigonal squashing, other types of (smaller) distortions and atomic displacements are present (the precise details are material dependent): rotations of the ligand octahedra with respect to each other, slight “dimerization” for part of the TM-TM links, displacements of the bridging ligands along the corresponding TM-TM contacts, etc. Therefore, even if the lattice parameters and interatomic distances are rescaled by the same percentage, given the slightly different environment seen by ions within

TABLE II. MRCI NN magnetic couplings (meV) for bond B2 in  $\text{Na}_2\text{IrO}_3$  for variable Ir-Ir bond length  $a$ .

$\delta a$	$a$ (Å)	$K$	$J$	$\Gamma_{xy}$	$\Gamma_{zx} = -\Gamma_{yz}$	$ K/J $
+2%	3.19	<b>-12.4</b>	<b>1.0</b>	-0.3	-3.0	12.40
Expt.	3.13	<b>-15.6</b>	<b>2.2</b>	-1.1	-0.8	7.09
-1.5%	3.08	<b>-18.2</b>	<b>3.1</b>	-1.4	-0.9	5.87
-3%	3.04	<b>-21.0</b>	<b>3.7</b>	-1.8	-1.3	5.68
-5%	2.97	<b>-25.6</b>	<b>4.8</b>	-2.5	-1.7	5.33

the B1 and B2 types of two-octahedra units, various matrix elements may be affected in a different manner. Consequently, we find for bond B2 a somewhat different behavior: While  $K$  evolves in a similar fashion as for bond B1,  $J$  becomes here twice the value at ambient pressure for the shortest Ir-Ir bond length considered.  $|K/J|$  decreases then with interatomic distance reduction (see Table II). However, the  $|K/J|$  ratio jumps from 7 at ambient pressure to 12.4 for 2% elongation of the Ir-Ir bond. Such increased bond lengths could be realized under tensile strain. The steep rise of the  $|K/J|$  ratio can be understood as a result of the rapid downturn of the Heisenberg  $J$  towards 0. In fact, the decreasing trend in  $J$  suggests that it would completely vanish with further slight elongation of the bonds, resulting in a purely anisotropic Hamiltonian.

The variations of the NN magnetic exchange interactions for  $\alpha\text{-RuCl}_3$ , as obtained by spin-orbit MRCI calculations, are listed in Table III:  $K$  remains ferromagnetic and increases in magnitude to -11.4 meV on 5% reduction of the Ru-Ru distance, as compared to the value of -5.6 meV at ambient pressure;  $J$  changes to 2.8 meV from a value of 1.2 meV at normal pressure. An interesting point to note is again the reduction of  $J$  towards zero with 2% elongation of the Ru-Ru bond. Also in this material, the  $|K/J|$  ratio reaches therefore the largest value for stretched bonds. A strong dependence on interatomic distances is further displayed by  $\Gamma_{xy}$  and  $\Gamma_{zx}$  but these effective parameters are never larger than 25% of  $K$  in  $\text{RuCl}_3$ . In contrast, in  $\beta\text{-Li}_2\text{IrO}_3$ ,  $\Gamma_{xy}$  becomes as large as half the value of  $K$  and twice the value of  $J$  for the shortest Ir-Ir distance considered for bond B2 (see Tables IV and V). This large  $\Gamma_{xy}$  stands out while comparing trends with other honeycomb systems.

All NN magnetic couplings computed for  $\beta\text{-Li}_2\text{IrO}_3$  are listed in Tables IV and V. For the case of B2 links in  $\beta\text{-Li}_2\text{IrO}_3$ ,  $K$  rises to -17.7 meV on 5% cutback in the Ir-Ir distance, an increase by nearly 50% as compared to -12.2 meV at ambient pressure.  $J$ , on the other hand, changes from -2.1 meV at ambient conditions to a value of -3.8 meV.

TABLE III. MRCI NN magnetic couplings (meV) in  $\text{RuCl}_3$  for variable Ru-Ru bond length  $a$ .

$\delta a$	$a$ (Å)	$K$	$J$	$\Gamma_{xy}$	$\Gamma_{zx} = -\Gamma_{yz}$	$ K/J $
+2%	3.52	<b>-4.5</b>	<b>0.7</b>	-1.0	-0.3	6.43
Expt.	3.45	<b>-5.6</b>	<b>1.2</b>	-1.2	-0.7	4.67
-1.5%	3.40	<b>-7.1</b>	<b>1.8</b>	-1.3	-0.9	3.94
-3%	3.35	<b>-8.7</b>	<b>2.3</b>	-1.6	-1.2	3.78
-5%	3.28	<b>-11.4</b>	<b>2.8</b>	-2.0	-1.8	4.07

TABLE IV. MRCI NN magnetic couplings (meV) for bond B1 in  $\beta$ -Li<sub>2</sub>IrO<sub>3</sub> for variable Ir-Ir bond length  $a$ .  $\mathbf{D} = (D, D, 0)$ .

$\delta a$	$a$ (Å)	$K$	$J$	$D$	$\Gamma_{xy}$	$ K/J $
+2%	3.04	<b>-12.21</b>	<b>0.20</b>	0.27	-1.50	61.05
Expt.	2.98	<b>-14.78</b>	<b>-0.26</b>	0.35	-2.08	56.85
-3%	2.89	<b>-17.01</b>	<b>-0.41</b>	0.45	-3.48	41.49
-5%	2.83	<b>-20.72</b>	<b>-0.60</b>	0.56	-4.80	34.53

Similar to the other compounds, the  $|K/J|$  ratio is maximal for positive bond-length increments.  $J$  even changes sign for 2% increase of the Ir-Ir distance for bond B1, which suggests that applying a very modest amount of tensile strain might also in this case bring the system close to the  $J = 0$  limit, where only the anisotropic couplings are finite. Vanishing  $|J/K|$  ratios were also predicted to occur in honeycomb iridates by adjusting the Ir-O-Ir bond angles [23]; similarly, vanishing  $J/D$  ratios were predicted for particular bond angles in pyrochlore iridates [43].

It is worth noting that the negative  $\Gamma$ 's shown here are consistent with the positive  $\Gamma$ 's obtained by other approaches [28,50], as the frames used to express these couplings differ by a rotation of 180° about the  $x$  axis. Density functional calculations also suggest a dominant  $K$  for  $\beta$ -Li<sub>2</sub>IrO<sub>3</sub> but provide somewhat larger  $\Gamma_{xy}$  values [33] as compared to the quantum-chemistry data.

To determine the order of the exponential dependence of  $K$  as a function of changes in the TM-TM distance, the trends shown in the tables were fitted to the function  $K = K_0 x^n$ , where  $K_0$  represents the Kitaev exchange amplitude at ambient pressure and  $n$  refers to the exponent of fractional change in the TM-TM distance, i.e.,  $x = a/a_0 = 1 + \delta a$ . The plots shown in Fig. 2 display the variations of  $K$ ,  $J$ , and  $\Gamma_{xy}$  in Na<sub>2</sub>IrO<sub>3</sub> and  $\alpha$ -RuCl<sub>3</sub> (shown together with the corresponding fits). The exponents obtained by such approximate fits over the whole  $\delta a$  range in  $\alpha$ -RuCl<sub>3</sub> are not far from the values predicted by the qualitative superexchange model; looking however at a smaller scale, it is seen (Table III) that the  $K/J$  ratio has a more subtle evolution. The lower  $n$  values for Na<sub>2</sub>IrO<sub>3</sub> and  $\beta$ -Li<sub>2</sub>IrO<sub>3</sub> point again to the changing nature of the exchange processes with slight modification of the surroundings, such as having different bond angles and ligand charges.

The all-important question is now whether these changes can stabilize the Kitaev spin liquid. Although  $K$ - $J$ - $\Gamma$  models are extensively studied, only very few works have accounted for bond inequivalence [20,48]. Nonetheless, to obtain an approximate answer we matched the changes of the coupling

TABLE V. MRCI NN magnetic couplings (meV) for bond B2 in  $\beta$ -Li<sub>2</sub>IrO<sub>3</sub> for variable Ir-Ir bond length  $a$ .

$\delta a$	$a$ (Å)	$K$	$J$	$\Gamma_{xy}$	$\Gamma_{zx} = -\Gamma_{yz}$	$ K/J $
+2%	3.03	<b>-11.7</b>	<b>-0.8</b>	-3.2	-0.7	14.63
Expt.	2.97	<b>-12.2</b>	<b>-2.1</b>	-4.1	-1.0	5.81
-1.5%	2.93	<b>-14.1</b>	<b>-2.7</b>	-4.9	-1.1	5.22
-3%	2.88	<b>-15.6</b>	<b>-3.2</b>	-6.1	-1.3	4.88
-5%	2.82	<b>-17.7</b>	<b>-3.8</b>	-8.1	-1.7	4.66

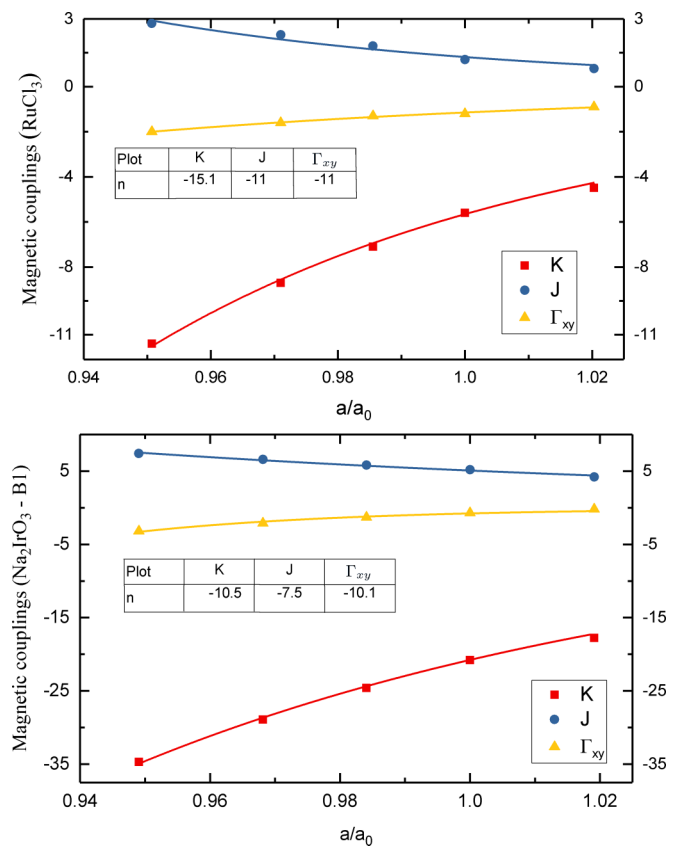


FIG. 2. NN couplings for variable TM-TM bond length, fitted to functions of the type  $A = A_0 x^n$  with  $x = a/a_0$ ; plots for  $\alpha$ -RuCl<sub>3</sub> (top) and for link B1 in Na<sub>2</sub>IrO<sub>3</sub> (bottom). Analogous plots for link B2 in Na<sub>2</sub>IrO<sub>3</sub> are provided in the Supplemental Material [49].

constants with the phase diagram of Rau *et al.* [24] and checked how the ground state of a model with B1 (B2) bonds only would change. Quite generally, we find that whenever  $|K/J|$  increases the ground state appears to be much closer to the QSL phase. For Na<sub>2</sub>IrO<sub>3</sub>, we actually find that bond B2 under 2% strain might be even located within the QSL phase and bond B1 very close to it.

*Summary.* We have employed advanced quantum-chemistry methods to model the effects of uniform pressure and strain on the exchange couplings in iridium and ruthenium compounds with honeycomb and related lattices. The obtained results demonstrate that the Kitaev, Heisenberg, symmetric off-diagonal, and antisymmetric anisotropic magnetic interactions stemming from the different exchange processes renormalize differently under volume change. By introducing external pressure or strain on actual materials one could therefore experimentally explore the rich theoretical phase diagram composed of the quantum-spin liquid, collinear, as well as noncollinear ordered states. For the honeycomb compounds, we find that moderate values of strain are most promising for pushing the ground state into the Kitaev spin-liquid region. We believe that the present results will motivate further strain experiments on Kitaev materials.

*Acknowledgments* This work was supported by the DFG (DE) through SFB 1143. G.J., S.R., and J.v.d.B. benefited from the facilities of the KITP. G.J. was supported in part by

the NSF under Grant No. NSF PHY11-25915. R.Y. and L.H. acknowledge Ulrike Nitzsche for technical support and the High Performance Computing Center (ZIH) of TU Dresden

for access to computational facilities. S.R. acknowledges support from an Australian Research Council Future Fellowship (FT180100211).

- 
- [1] L. Balents, *Nature (London)* **464**, 199 (2010).
- [2] T.-H. Han, J. S. Helton, S. Chu, D. G. Nocera, J. A. Rodriguez-Rivera, C. Broholm, and Y. S. Lee, *Nature (London)* **492**, 406 (2012).
- [3] M. Yamashita, N. Nakata, Y. Senshu, M. Nagata, H. M. Yamamoto, R. Kato, T. Shibauchi, and Y. Matsuda, *Science* **328**, 1246 (2010).
- [4] A. Kitaev, *Ann. Phys.* **321**, 2 (2006).
- [5] S. M. Albrecht, A. P. Higginbotham, M. Madsen, F. Kuemmeth, T. S. Jespersen, J. Nygård, P. Krogstrup, and C. M. Marcus, *Nature (London)* **531**, 206 (2016).
- [6] G. Jackeli and G. Khaliullin, *Phys. Rev. Lett.* **102**, 017205 (2009).
- [7] J. Chaloupka, G. Jackeli, and G. Khaliullin, *Phys. Rev. Lett.* **105**, 027204 (2010).
- [8] Y. Singh and P. Gegenwart, *Phys. Rev. B* **82**, 064412 (2010).
- [9] F. Ye, S. Chi, H. Cao, B. C. Chakoumakos, J. A. Fernandez-Baca, R. Custelcean, T. F. Qi, O. B. Korneta, and G. Cao, *Phys. Rev. B* **85**, 180403 (2012).
- [10] Y. Singh, S. Manni, J. Reuther, T. Berlijn, R. Thomale, W. Ku, S. Trebst, and P. Gegenwart, *Phys. Rev. Lett.* **108**, 127203 (2012).
- [11] S. K. Choi, R. Coldea, A. N. Kolmogorov, T. Lancaster, I. I. Mazin, S. J. Blundell, P. G. Radaelli, Y. Singh, P. Gegenwart, K. R. Choi, S.-W. Cheong, P. J. Baker, C. Stock, and J. Taylor, *Phys. Rev. Lett.* **108**, 127204 (2012).
- [12] K. A. Modic, T. E. Smidt, I. Kimchi, N. P. Breznay, A. Biffin, S. Choi, R. D. Johnson, R. Coldea, P. Watkins-Curry, G. T. McCandless, J. Y. Chan, F. Gandara, Z. Islam, A. Vishwanath, A. Shekhter, R. D. McDonald, and J. G. Analytis, *Nat. Commun.* **5**, 4203 (2014).
- [13] T. Takayama, A. Kato, R. Dinnebier, J. Nuss, H. Kono, L. S. I. Veiga, G. Fabbri, D. Haskel, and H. Takagi, *Phys. Rev. Lett.* **114**, 077202 (2015).
- [14] S. H. Chun, J.-W. Kim, J. Kim, H. Zheng, C. C. Stoumpos, C. D. Malliakas, J. F. Mitchell, K. Mehlawat, Y. Singh, Y. Choi, T. Gog, A. Al-Zein, M. M. Sala, M. Krisch, J. Chaloupka, G. Jackeli, G. Khaliullin, and B. J. Kim, *Nat. Phys.* **11**, 462 (2015).
- [15] R. D. Johnson, S. C. Williams, A. A. Haghighirad, J. Singleton, V. Zapf, P. Manuel, I. I. Mazin, Y. Li, H. O. Jeschke, R. Valentí, and R. Coldea, *Phys. Rev. B* **92**, 235119 (2015).
- [16] L. J. Sandilands, Y. Tian, K. W. Plumb, Y.-J. Kim, and K. S. Burch, *Phys. Rev. Lett.* **114**, 147201 (2015).
- [17] L. J. Sandilands, Y. Tian, A. A. Reijnders, H.-S. Kim, K. W. Plumb, Y.-J. Kim, H.-Y. Kee, and K. S. Burch, *Phys. Rev. B* **93**, 075144 (2016).
- [18] A. Banerjee, C. A. Bridges, J.-Q. Yan, A. A. Aczel, L. Li, M. B. Stone, G. E. Granroth, M. D. Lumsden, Y. Yiu, J. Knolle, S. Bhattacharjee, D. L. Kovrizhin, R. Moessner, D. A. Tennant, D. G. Mandrus, and S. E. Nagler, *Nat. Mater.* **15**, 733 (2016).
- [19] A. Banerjee, J. Yan, J. Knolle, C. A. Bridges, M. B. Stone, M. D. Lumsden, D. G. Mandrus, D. A. Tennant, R. Moessner, and S. E. Nagler, *Science* **356**, 1055 (2017).
- [20] V. M. Katukuri, S. Nishimoto, V. Yushankhai, A. Stoyanova, H. Kandpal, S. Choi, R. Coldea, I. Rousochatzakis, L. Hozoi, and J. van den Brink, *New J. Phys.* **16**, 013056 (2014).
- [21] V. M. Katukuri, R. Yadav, L. Hozoi, S. Nishimoto, and J. van den Brink, *Sci. Rep.* **6**, 29585 (2016).
- [22] R. Yadav, N. A. Bogdanov, V. M. Katukuri, S. Nishimoto, J. van den Brink, and L. Hozoi, *Sci. Rep.* **6**, 37925 (2016).
- [23] S. Nishimoto, V. M. Katukuri, V. Yushankhai, H. Stoll, U. K. Röbler, L. Hozoi, I. Rousochatzakis, and J. van den Brink, *Nat. Commun.* **7**, 10273 (2016).
- [24] J. G. Rau, E. K.-H. Lee, and H.-Y. Kee, *Phys. Rev. Lett.* **112**, 077204 (2014).
- [25] Y. Yamaji, Y. Nomura, M. Kurita, R. Arita, and M. Imada, *Phys. Rev. Lett.* **113**, 107201 (2014).
- [26] H.-S. Kim, V. Shankar, A. Catuneanu, and H.-Y. Kee, *Phys. Rev. B* **91**, 241110(R) (2015).
- [27] S. M. Winter, A. A. Tsirlin, M. Daghofer, J. van den Brink, Y. Singh, P. Gegenwart, and R. Valentí, *J. Phys.: Condens. Matter* **29**, 493002 (2017).
- [28] S. M. Winter, Y. Li, H. O. Jeschke, and R. Valentí, *Phys. Rev. B* **93**, 214431 (2016).
- [29] L. S. I. Veiga, M. Etter, K. Glazyrin, F. Sun, C. A. Escanhoela, G. Fabbri, J. R. L. Mardegan, P. S. Malavi, Y. Deng, P. P. Stavropoulos, H.-Y. Kee, W. G. Yang, M. van Veenendaal, J. S. Schilling, T. Takayama, H. Takagi, and D. Haskel, *Phys. Rev. B* **96**, 140402 (2017).
- [30] N. P. Breznay, A. Ruiz, A. Frano, W. Bi, R. J. Birgeneau, D. Haskel, and J. G. Analytis, *Phys. Rev. B* **96**, 020402 (2017).
- [31] Z. Wang, J. Guo, F. F. Tafti, A. Hegg, S. Sen, V. A. Sidorov, L. Wang, S. Cai, W. Yi, Y. Zhou, H. Wang, S. Zhang, K. Yang, A. Li, X. Li, Y. Li, J. Liu, Y. Shi, W. Ku, Q. Wu, R. J. Cava, and L. Sun, *Phys. Rev. B* **97**, 245149 (2018).
- [32] G. Bastien, G. Garbarino, R. Yadav, F. J. Martinez-Casado, R. Beltrán Rodríguez, Q. Stahl, M. Kusch, S. P. Limandri, R. Ray, P. Lampen-Kelley, D. G. Mandrus, S. E. Nagler, M. Roslova, A. Isaeva, T. Doert, L. Hozoi, A. U. B. Wolter, B. Büchner, J. Geck, and J. van den Brink, *Phys. Rev. B* **97**, 241108 (2018).
- [33] M. Majumder, R. S. Manna, G. Simutis, J. C. Orain, T. Dey, F. Freund, A. Jesche, R. Khasanov, P. K. Biswas, E. Bykova, N. Dubrovinskaia, L. S. Dubrovinsky, R. Yadav, L. Hozoi, S. Nishimoto, A. A. Tsirlin, and P. Gegenwart, *Phys. Rev. Lett.* **120**, 237202 (2018).
- [34] M. Jenderka, J. Barzola-Ququia, Z. Zhang, H. Frenzel, M. Grundmann, and M. Lorenz, *Phys. Rev. B* **88**, 045111 (2013).
- [35] S. Rachel, L. Fritz, and M. Vojta, *Phys. Rev. Lett.* **116**, 167201 (2016).
- [36] B. Perreault, S. Rachel, F. J. Burnell, and J. Knolle, *Phys. Rev. B* **95**, 184429 (2017).

- [37] K. Kitagawa, T. Takayama, Y. Matsumoto, A. Kato, R. Takano, Y. Kishimoto, S. Bette, R. Dinnebier, G. Jackeli, and H. Takagi, *Nature (London)* **554**, 341 (2018).
- [38] I. Rousochatzakis and N. B. Perkins, *Phys. Rev. Lett.* **118**, 147204 (2017).
- [39] J. Chaloupka, G. Jackeli, and G. Khaliullin, *Phys. Rev. Lett.* **110**, 097204 (2013).
- [40] W. A. Harrison, *Electronic Structure and the Properties of Solids: The Physics of the Chemical Bond* (Dover Publications, NY, 1989).
- [41] For both types of NN TM-TM links, B1 and B2.
- [42] N. A. Bogdanov, V. M. Katukuri, J. Romhányi, V. Yushankhai, V. Kataev, B. Büchner, J. van den Brink, and L. Hozoi, *Nat. Commun.* **6**, 7306 (2015).
- [43] R. Yadav, M. Pereiro, N. A. Bogdanov, S. Nishimoto, A. Bergman, O. Eriksson, J. van den Brink, and L. Hozoi, *Phys. Rev. Materials* **2**, 074408 (2018).
- [44] H. B. Cao, A. Banerjee, J.-Q. Yan, C. A. Bridges, M. D. Lumsden, D. G. Mandrus, D. A. Tennant, B. C. Chakoumakos, and S. E. Nagler, *Phys. Rev. B* **93**, 134423 (2016).
- [45] M. Minola, L. Hozoi, D. Di Castro, R. Felici, M. Moretti Sala, A. Tebano, G. Balestrino, G. Ghiringhelli, J. van den Brink, and L. Braicovich, *Phys. Rev. B* **87**, 085124 (2013).
- [46] V. Hermann, M. Altmeyer, J. Ebad-Allah, F. Freund, A. Jesche, A. A. Tsirlin, M. Hanfland, P. Gegenwart, I. I. Mazin, D. I. Khomskii, R. Valentí, and C. A. Kuntscher, *Phys. Rev. B* **97**, 020104 (2018).
- [47] T. Helgaker, P. Jørgensen, and J. Olsen, *Molecular Electronic-Structure Theory* (Wiley, Chichester, 2000).
- [48] P. Lampen-Kelley, S. Rachel, J. Reuther, J.-Q. Yan, A. Banerjee, C. Bridges, H. Cao, S. Nagler, and D. Mandrus, *Phys. Rev. B* **98**, 100403(R) (2018).
- [49] See Supplemental Material at <http://link.aps.org/supplemental/10.1103/PhysRevB.98.121107> for additional computational details, which also includes Refs. [51–55].
- [50] L. Janssen, E. C. Andrade, and M. Vojta, *Phys. Rev. B* **96**, 064430 (2017).
- [51] D. Figgen, K. A. Peterson, M. Dolg, and H. Stoll, *J. Chem. Phys.* **130**, 164108 (2009).
- [52] K. A. Peterson, D. Figgen, M. Dolg, and H. Stoll, *J. Chem. Phys.* **126**, 124101 (2007).
- [53] T. H. Dunning, *J. Chem. Phys.* **90**, 1007 (1989).
- [54] D. E. Woon and T. H. Dunning, *J. Chem. Phys.* **98**, 1358 (1993).
- [55] K. Pierloot, B. Dumez, P.-O. Widmark, and B. O. Roos, *Theor. Chim. Acta* **90**, 87 (1995).